Compton Polarimeter for Qweak Experiment at Jefferson Laboratory

by

David Zou

Submitted to the Department of Physics
in partial fulfillment of the requirements for the degree of

Bachelor of Science in Physics

at the

MASSACHUSETTS INSTITUTE OF TECHNOLOGY

June 2011

Author .....
Department of Physics
May 13, 2011

Certified by. .....
Stanley Kowalski
Professor of Physics
Thesis Supervisor

Accepted by ....
Professor Nergis Mavalvala
Senior Thesis Coordinator, Department of Physics

Compton Polarimeter for Qweak Experiment at Jefferson Laboratory

by

David Zou

Submitted to the Department of Physics
on May 13, 2011, in partial fulfillment of the
requirements for the degree of
Bachelor of Science in Physics

Abstract

The Q_{weak} experiment at Jefferson Lab aims to make the first precision measurement of the proton's weak charge, $Q_W^p = 1 - 4\sin^2\theta_W$ at $Q^2 = 0.026\text{GeV}^2$. Given the precision goals in the Q_{weak} experiment, the electron beam polarization must be known to an absolute uncertainty of 1%. A new Compton polarimeter has been built and installed in Hall C in order to make this important measurement. Compton polarimetry has been chosen for its ability to deliver continuous on-line measuremnts at high currents necessary for Q_{weak} (up to $180\mu A$). In this thesis, we collected and analyzed electron beam polarization data using the Q_{weak} Compton polarimeter. Currently, data from the Compton can already be used to calculate preliminary values of experimental physics asymmetries and also the electron beam polarization. These preliminary results are promising indications that Q_{weak} will be able to meet its stated precision goals.

Thesis Supervisor: Stanley Kowalski
Title: Professor of Physics

Acknowledgments

I would like to thank my thesis advisor, Professor Stanley Kowalski who first brought me into the Q_{weak} project as his UROP student, and has assisted me greatly in the process of writing this thesis, generously providing advice, feedback, and materials throughout the entirety of the process. I would also like to thank Professor Wouter Deconinck who supervised my research with the Q_{weak} project and greatly assisted me in finding documentation as well. I thank Don Jones and Mark Dalton, whose analysis and help provided many of the plots included in this thesis. I would like to thank David Gaskell and Ernie Ihloff for helping me in providing information on various chicane parameters. Finally, I would like to thank all the members of the Q_{weak} collaboration whose work has allowed the Q_{weak} experiment to advance as far as it has, and whose names and roles I have not included in this acknowledgment.

Contents

Chapter 1

Introduction

The Q_{weak} experiment [1] in Hall C at Jefferson Lab in Newport News, Virginia aims to make the first precision measurement of the proton's weak charge, $Q_W^p = 1 - 4\sin^2\theta_W$. The proton has a weak charge that causes a very small effect that can be observed in the elastic scattering of polarized electrons on protons. A small asymmetry of 270 ppb can be identified in the number of detected particles for the two electron polarization states. Q_{weak} plans to make high precision measurements of the parity-violating asymmetry in elastic ep scattering at $Q^2 = 0.026GeV^2$ using a 85% CW polarized beam with a current of 180 μA on a 35 cm liquid hydrogen target. The setup provides sensitivities capable of determining the proton's weak charge with 4% combined statistical and systematic uncertainty, an accuracy capable of searching for physics beyond the Standard Model. This measurement is sensitive to Standard Model physics at energies up to 3TeV. Given the low statistical and systematic errors in the Q_W^p measurement, Q_{weak} agreement with Standard Model predictions would produce new relevant constraints on possible extensions beyond the Standard Model (see Section 1.2 of [1] for details). These measurements will also provide an independent measurement of the weak mixing angle $sin^2\theta_W$ with a precision of $\approx 0.3\%$, the most precise low Q^2 measurement of the weak mixing angle to date (See Figure $1-1$).

The Continuous Electron Beam Accelerator Facility (CEBAF) at Jefferson Laboratory delivers a continuous electron beam with an energy between 0.8 and 6.0 GeV

to three experimental halls. Measurements of the electron polarization necessary for Q_{weak} requires an absolute uncertainty of 1% in order to meet the experimental error goals (See Table 1.1). In Hall C, a Compton polarimeter is used to make this important measurement. The polarimeter works by using Compton scattering by colliding a green laser beam with the electron beam while detecting and measuring the energy of the resulting scattered photons and scattered electrons. The counting rate asymmetry between the two beam polarization states depends on the interaction kinematics and the beam polarization.

In Hall C, previous experiments, such as G0, have made similar measurements using a Møller polarimeter, whose operation and behavior is now well understood. However, even after upgrades, the Møller polarimeter could only operate at currents below $8\mu A$. A new Compton polarimeter has been built for the Q_{weak} experiment, which is capable of measuring beam polarization at full current (up to $180\mu A$). The Compton polarimeter also has the advantage of providing continuous on-line measurements, whereas Møller polarimeter measurements destroys the beam properties and cannot operate simulaneously with data collection.

This thesis will cover the physics involved in the Compton polarimeter, briefly describe the experimental setup and relevant hardware, and present preliminary measurements of energy-weighted asymmetry and the electron beam polarization.

Source of error	Contribution to $\Delta A_{phys}/A_{phys}$	Contribution to $\Delta Q_W^p/Q_W^p$
Counting Statistics	2.1%	3.2%
Hadronic structure	–	1.5%
Beam polarimetry	1.0%	1.5%
Absolute Q^2	0.5%	1.0%
Backgrounds	0.5%	0.7%
Helicity-correlated beam properties	0.5%	0.7%
TOTAL:	2.5%	4.1%

Table 1.1: Table summarizing the total anticipated statistical and systematic error contributions to the physics asymmetry and the extracted Q_W^p measurements. Table taken from the Q_{weak} experiment proposal [1].

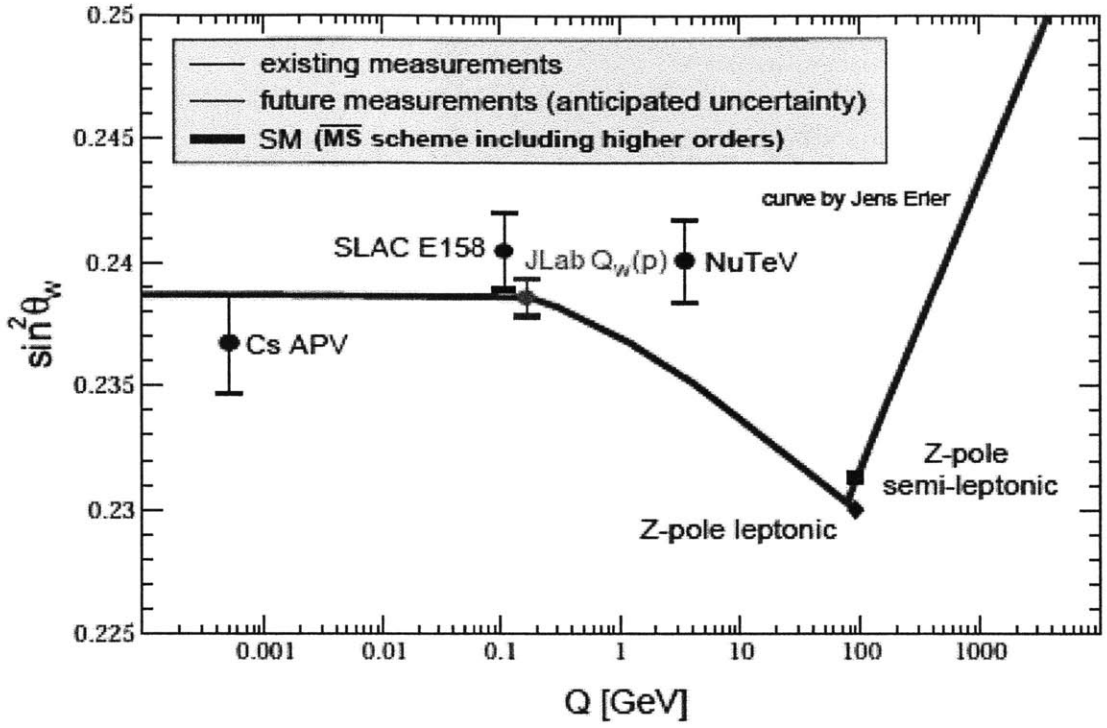

Figure 1-1: Calculated values of the predicted weak mixing angle based on the Standard Model. The black error bars show measurements from previous experiments. The JLab Q_W^p data point shows the proposed 4% Q_{weak} measurement. Note that the vertical location of the JLab Q_W^p point is arbitrarily chosen and does not reflect real data. The existing data points were measured from atomic parity violation (APV) [11], SLAC E-158 [12], deep inelastic neutrino-nucleus scattering (NuTeV) [13], and Z^0 pole asymmetries (LEP+SLC) [14]. The curve was generated by Jens Erier and this figure was taken from [1].

Chapter 2

Compton Scattering

The physics and kinematics of Compton scattering greatly influences our setup. In this section we will discuss the measurement of electron polarization by Compton scattering, review the basic kinematics of Compton scattering, and give a brief summary of the dynamics, including polarized and unpolarized cross sections and longitudinal asymmetry.

2.1 Electron Polarization by Compton Scattering

The longitudinal polarization of the electron beam P_e with respect to the z axis is defined by

$$P_e = \frac{N_e^+ - N_e^-}{N_e^+ + N_e^-} \tag{2.1}$$

where $N_e^\pm$ is the number of electrons with spin $s_z^e = \pm\frac{1}{2}$ respectively. With a total number of electrons $N_e = N_e^+ + N_e^-$, one has the following relations

$$N_e^\pm = \frac{N_e}{2}(1 \pm P_e) \tag{2.2}$$

In a Compton Polarimeter, one extracts the longitudinal polarization P_e of the electron bream from the measurement of the experimental asymmetry A_{exp} from the scattering of a circularly polarized photon beam with the polarized electron beam. Given a photon beam polarization P_γ one has the following relations

$$A_{exp} = \frac{n^+ - n^-}{n^+ + n^-} = P_e P_\gamma A_l \tag{2.3}$$

where n^+ and n^- are the number of Compton scattering events before and after a reversal of the electron polarization ($P_e \to -P_e$) respectively. Here, the experimental asymmetry A_{exp} is related to the known theroretical asymmetry A_l for Compton scattering for electron and photon with parallel spin $\sigma^{\rightarrow}_{\Rightarrow}$ and anti-parallel spin $\sigma^{\leftarrow}_{\Rightarrow}$ and given by,

$$A_l = \frac{\sigma^{\rightarrow}_{\Rightarrow} - \sigma^{\leftarrow}_{\Rightarrow}}{\sigma^{\rightarrow}_{\Rightarrow} + \sigma^{\leftarrow}_{\Rightarrow}} \tag{2.4}$$

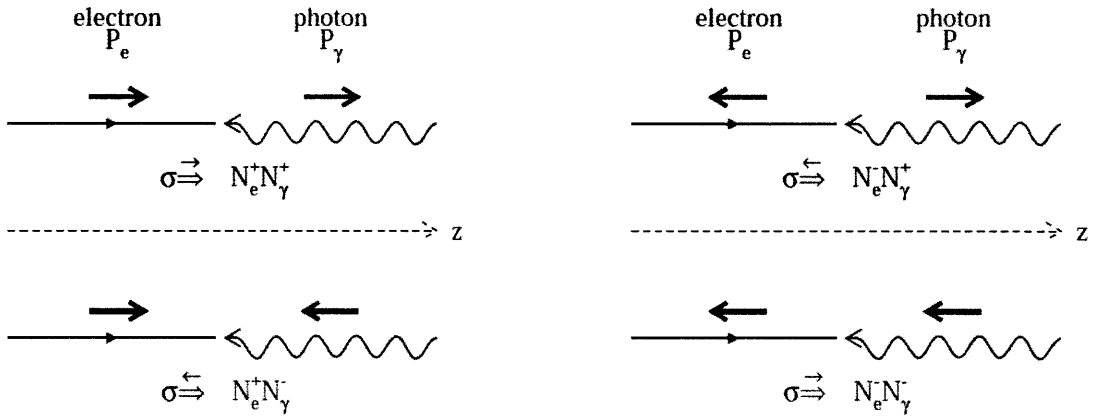

Figure 2-1: Possible helicity configurations.Electron and photon polarizations are defined with respect to the z axis

2.2 Kinematics of Compton Scattering

A basic diagram of a Compton scattering event is depicted in 2-2. Note the following characterisitcs of the interaction:

- Incident electron e has energy E and momentum $\vec{p} = (0, 0, p)$ along the z axis,
- Incident photon γ has energy k and momentum $\vec{k} = (0, -k\sin\alpha_c, -k\cos\alpha_c)$ along the z axis,

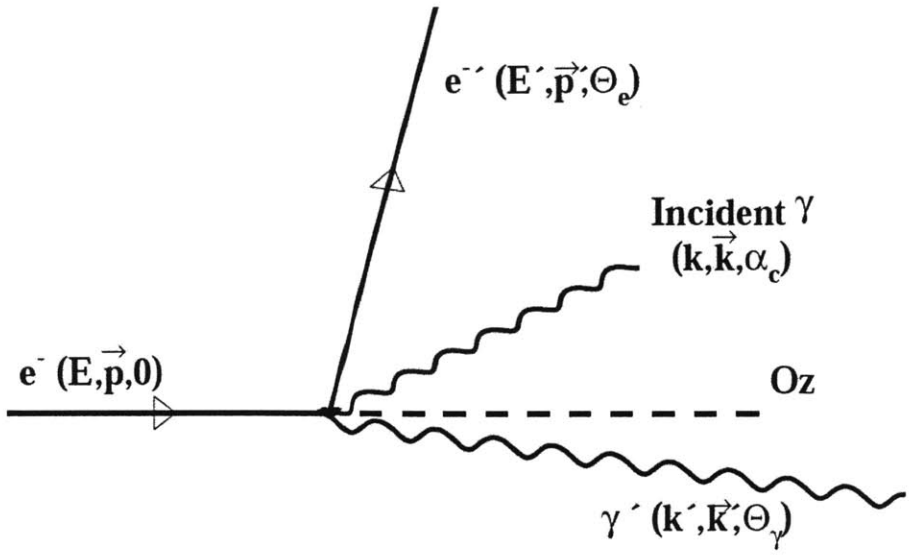

Figure 2-2: Compton Scattering $e\gamma \rightarrow e\gamma$

- Scattered electron e' has energy E', scattering angle θ_e, and a momentum $\vec{p'} = (p' \sin\theta_e \sin\phi, p' \sin\theta_e \cos\phi, p' \cos\theta_e)$,
- Scattered photon γ' has energy k', scattering angle θ_γ, and a momentum $\vec{k'} = (k' \sin\theta_\gamma \sin\phi, k' \sin\theta_\gamma \cos\phi, k' \cos\theta_\gamma)$,

Note that ϕ is the angle between the incident and scattering planes, but will not be relevant in our calculations. Therefore, only one parameter will be necessary to determine the whole kinematic if the initial state in this 2-body kinematics is known. From these kinematics, we derive a relationship between the scattered photon energy k' and the scattered photon angle θ_γ. Note that for the remainder of this document, equations will be expressed in natural units ($c = \hbar = 1$):

$$k' = k\frac{E + p\cos\alpha_c}{E + k - p\cos\theta_\gamma + k\cos(\alpha_c - \theta_\gamma)} \tag{2.5}$$

Using $\gamma = E/m$, the equation may be simplified for a photon incident angle $\alpha_c = 0$,

$$k' \approx k\frac{4a\gamma^2}{1 + a\theta_\gamma^2\gamma^2} \tag{2.6}$$

where

$$a = \frac{1}{1 + \frac{4k\gamma}{m}} = \frac{1}{1 + \frac{4kE}{m^2}} \tag{2.7}$$

At $\theta_\gamma = 0$, k' and E' are respectively maximized and minimized.

$$k'_{max} = 4ak\gamma^2 = 4ak\frac{E^2}{m^2} \tag{2.8}$$

$$E'_{min} = E + k - k'_{max} = E + k - 4ak\frac{E^2}{m^2} \approx E - 4ak\frac{E^2}{m^2} \tag{2.9}$$

while at $\theta_\gamma = \pi$, one sees the opposite case: k' and E' are respectively minimized and maximized.

$$k'_{min} = k \tag{2.10}$$

$$E'_{max} = E + k - k'_{min} = E \tag{2.11}$$

The scattered electron momentum p' is related to the scattered electron angle θ_e by a second order equation:

$$p'^2(C^2 - B^2) - 2AB_p{}' + m^2C^2 - A^2 = 0, \tag{2.12}$$

$$p'=\frac{AB \pm C\sqrt{A^2 - m^2(C^2 - B^2)}}{C^2 - B^2} \tag{2.13}$$

where

$$\begin{aligned} A &= m^2 + Ek + kp\cos\alpha_c \\ B &= p\cos\theta_e - k\cos(\theta_e - \alpha_c) \\ C &= E + k \end{aligned} \tag{2.14}$$

One obtains the maximum electron angle θ_e^{max} when $A^2 = m^2(C^2 - B^2)$. For small incident photon angle and energy,

$$\theta_e^{max} \approx 2\frac{k}{m} \tag{2.15}$$

In Q_{weak}, scattered electrons and photons have a small opening angle. In order to separate scattered electrons, scattered photons, and incident electrons for detection, Q_{weak} uses a magnetic chicane. The magnetic chicane deflects and separates the scattered and incident electrons, leaving room for the laser and photon detector.

2.3 Scattering Cross Section and Asymmetry

The differential unpolarized Compton scattering cross section is given by [7]:

$$\frac{d\sigma}{d\rho} = 2\pi r_0^2 a\left(\frac{\rho^2(1-a)^2}{1-\rho(1-a)} + 1 + \left(\frac{1-\rho(1+a)}{1-\rho(1-a)}\right)^2\right) \tag{2.16}$$

where the classical electron radius $r_0 = \alpha_c \hbar c/mc^2 = 2.817 \times 10^{-13}$ cm, $\rho = \frac{k'}{k'_{max}}$ is the scattered photon energy normalized to the maximal energy (see Eq. 2.8), and a is the kinematic parameter given in Eq. 2.7: $a = 1/(1 + \frac{4kE}{m^2})$. k'_{max} has a calculable value at the Compton edge of the laser-electron beam interaction.

Integrating Eq. 2.16 gives the total scattering cross section

$$\sigma = \pi r_0^2 a \frac{-1 - 14a + 16a^2 - 2a^3 + a^4 + 2\ln(a) - 12\ln(a)a - 6\ln(a)a^2}{(1-a)^3} \tag{2.17}$$

The longitudinal differential asymmetry is given by

$$A_l = \frac{\sigma^{\rightarrow}_{\Rightarrow} - \sigma^{\leftarrow}_{\Rightarrow}}{\sigma^{\rightarrow}_{\Rightarrow} + \sigma^{\leftarrow}_{\Rightarrow}} = \frac{2\pi r_0^2 a}{d\sigma/d\rho}(1 - \rho(1+a))[1 - \frac{1}{(1-\rho(1-a))^2}] \tag{2.18}$$

The longitudinal asymmetry A_l is maximized when $\rho = 1$, in order words, when the scattered photon energy is maximized ($k' = k'_{max}$) and the scattered electron

energy is minimized ($E' = E'_{min}$):

$$A_l^{max} = \frac{(1-a)(1+a)}{1+a^2} \tag{2.19}$$

It is important to note that the asymmetry A_l is related to the scattered photon energy. A_l is negative at low scattered photon energies, positive at higher energies, and is equal to zero for $\rho_0 = 1/(1+a)$. In other words, when

$$k'_0 = \frac{2k\gamma^2}{1+2\frac{k\gamma}{m}} \tag{2.20}$$

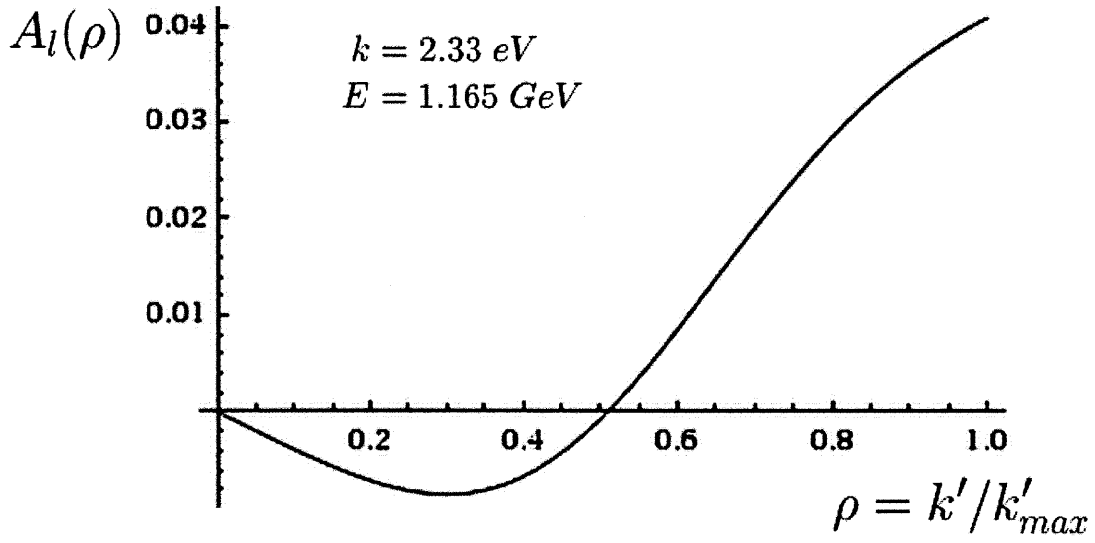

Figure 2-3: Theoretical photon asymmetry using Q_{weak} parameters. The asymmetry crosses zero at $\rho_0 \simeq 0.51$, when $k' = k'_0 \simeq 23.7$MeV (See Equation 2.20). The maximum value of the theoretical asymmetry (given at ρ =1) is 4.07E-2.

Chapter 3

Experimental Measurement of the Electron Polarization

The polarization of the electron beam is reversed at a rate of 1kHz and the reversal patterns of + - - + or - + + -, which are chosen pseudo-randomly. Q_{weak} extracts the longitudinal polarization P_e of the electron beam from the asymmetry between two measurements of Compton scattering with parallel (+) or anti-parallel (-) polarization of the electron and laser beams. The experiment considers three possible methods [5]:

- Differential Polarization Measurement

  The scattered photon or electron energy can be determined event by event. The numbers of Compton scattering events n_+^i and n_-^i are measured as a function of the scattered photon or electron energy in N_b bins. In each energy bin, a measurement of the polarization P_e^i is performed from the asymmetry of these numbers. The electron polarization is given by the weighted mean of P_e^i.

- Integrated Polarization Measurement

  Only the numbers of Compton scattering events integrated over the energy range N_+ and N_- are measured, without energy measurements of the scattered particles. The electron polarization can be deduced from the asymmetry of these

numbers. This is possible if the detection efficiency and the energy threshold for the scattered particles detected are known.

- Energy Polarization Weighted Measurement

  If only measurements of the energy integrated over a limited energy range is possible, the polarization can be deduced from the asymmetry between the integrated energies E_+ and E_-. In this case, Q_{weak} must know the detection efficiency and the energy threshold. The error also depends on these two parameters.

Each measurement is performed with a luminosity $\mathcal{L}_+(\mathcal{L}_-)$ during a time $T_+(T_-)$ and will be later normalized to this integrated luminosity. In the following sections, we will assume, for the two measurements with parallel (and anti-parallel) polarization of the electron and laser beams, the same differential efficiency

$$\epsilon_+(\rho) = \epsilon_-(\rho) = \epsilon(\rho) \tag{3.1}$$

and the same integrated luminosity

$$\mathcal{L}_+T_+ = \mathcal{L}_-T_- = \mathcal{L}T/2 \tag{3.2}$$

where $\mathcal{L}$ is the mean luminosity and T is the total time of the measurements.

3.1 Differential Polarization Measurement

The numbers of Compton scattering events as a function of the scattered photon energy for each of the N_b energy bins are

$$n_+^i = \mathcal{L}_+T_+ \int_{\rho_i}^{\rho_i+1} d\rho\ \epsilon_+(\rho)\ \frac{d\sigma}{d\rho}(\rho)(1 + P_eP_\gamma A_l(p)), \tag{3.3}$$

$$n_-^i = \mathcal{L}_-T_- \int_{\rho_i}^{\rho_i+1} d\rho\ \epsilon_-(\rho)\ \frac{d\sigma}{d\rho}(\rho)(1 - P_eP_\gamma A_l(p)), \tag{3.4}$$

where $\frac{d\sigma}{d\rho}$ is the unpolarized differential Compton cross section and $A_l(\rho)$ is the differential asymmetry.

The experimental asymmetry for each bin is related to the electron polarization by

$$A^i_{exp} = \frac{n^i_+ - n^i_-}{n^i_+ + n^i_-} = P_e P - \gamma \frac{\int d\rho\ \epsilon \frac{d\sigma}{d\rho} A_l}{\int d\rho\ \epsilon \frac{d\sigma}{d\rho}} = P_e P_\gamma < A_l >_i \approx P_e P_\gamma A^i_l \tag{3.5}$$

where A^i_l is the longitudinal polarization at the center of the bin.

The electron polarization measured for each bin P^i_e is given by

$$P^i_e = \frac{A^i_{exp}}{P_\gamma < A_l >_i} \approx \frac{A^i_{exp}}{P_\gamma A^i_l} \tag{3.6}$$

The electron polarization has an absolute error dP^i_e which is nearly independent of the detection efficiency given by

$$\frac{dP^{i2}_e}{P^{i2}_e} = \frac{1 - (P_e P_\gamma A^i_l)^2}{2n^i_t} \frac{1}{(P_e P_\gamma A^i_l)^2} \tag{3.7}$$

$$dP^{i2}_e = \frac{1}{\mathcal{L} T P^2_\gamma} \frac{1 - (P_e P_\gamma A^i_l)^2}{\sigma^i A^{i2}_l} \tag{3.8}$$

where n^i_t is the total number of events for the ith bin given by

$$n^i_t = n^i_+ + n^i_- = \mathcal{L} T \int_{\rho_i}^{\rho_i + 1} d\rho\ \epsilon\ \frac{d\sigma}{d\rho}(\rho) = \mathcal{L} T \sigma^i \tag{3.9}$$

The final electron polarization , obtained as the weighted mean of these polarization measurements, is then given by

$$P_e = \frac{\sum_{i=1}^{N_b} \frac{P^i_e}{dP^{i2}_e}}{\sum_{i=1}^{N_b} \frac{1}{dP^{i2}_e}} \tag{3.10}$$

and is also nearly independent of the detection efficiency and does not depend on the detection threshold.

For a total number of events N_t for an energy threshold ρ_{min}

$$N_t = \mathcal{L}T\sigma_t \; with \; \sigma_t = \int_{\rho_{min}}^{1} d\rho \; \epsilon \; \frac{d\sigma}{d\rho}(\rho) \tag{3.11}$$

the uncertainty achieved is given by

$$\frac{1}{dP_e{}^2} = \mathcal{L}TP_\gamma^2 \int_{\rho_{min}}^{1} \frac{\epsilon\sigma A_l{}^2}{1-(P_eP_\gamma A_l)^2} \tag{3.12}$$

$$(\frac{dP_e}{P_e})^2 = \mathcal{L}TP_e^2P_\gamma^2\sigma_t < \frac{A_l{}^2}{1-(P_eP_\gamma A_l)^2} > \approx \mathcal{L}TP_e^2P_\gamma^2\sigma_t < A_l^2 > \tag{3.13}$$

3.2 Integrated Polarization Measurement

The numbers of Compton scattering events integrated over the energy range N_+ and N_- are

$$N_+ = \mathcal{L}_+T_+ \int_{\rho_{min}}^{1} d\rho \; \epsilon_+(\rho) \; \frac{d\sigma}{d\rho}(\rho)(1+P_eP_\gamma A_l(p)), \tag{3.14}$$

$$N_- = \mathcal{L}_-T_- \int_{\rho_{min}}^{1} d\rho \; \epsilon_-(\rho) \; \frac{d\sigma}{d\rho}(\rho)(1-P_eP_\gamma A_l(p)), \tag{3.15}$$

The experimental integrated asymmetry is then related to the electron polarization by

$$A_{exp} = \; = P_eP_\gamma \frac{\int \epsilon\sigma A_l}{\int \epsilon\sigma} = P_eP_\gamma < A_l > \tag{3.16}$$

where the mean value $< A_l >$ is given by

$$< A_l >= \frac{\int_{\rho_{min}}^{1} d\rho \; \epsilon(\rho) \; \frac{d\sigma}{d\rho}(\rho) A_l(\rho)}{\int_{\rho_{min}}^{1} d\rho \; \epsilon(\rho) \; \frac{d\sigma}{d\rho}(\rho)} \tag{3.17}$$

The electron polarization is thus given by

$$P_e = \frac{A_{exp}}{P_\gamma < A_l >} \tag{3.18}$$

which, as shown, is proportional to the inverse of the mean longitudinal asymmetry

and therefore is dependent on the detection efficiency and on the detection threshold ρ_{min}.

The absolute and relative uncertainties on the experimental integrated asymmetry are

$$dA_{exp}^2 = \frac{1}{\mathcal{L}T}\frac{1}{\sigma_t}(1-(P_eP_\gamma < A_l >)^2), \tag{3.19}$$

$$(\frac{dA_{exp}}{A_{exp}})^{-2} = (\frac{dP_e}{P_e})^{-2} = \mathcal{L}TP_e^2P_\gamma^2\sigma_t\frac{< A_l >^2}{(1-(P_eP_\gamma < A_l >)^2)}, \tag{3.20}$$

where σ_t and N_t are given by equation 3.11.

3.3 Energy Weighted Polarization Measurement

The integrated energy E_+ and E_- over the energy range and over the time T are given by

$$E_+ = \mathcal{L}_+T_+\int_{\rho_{min}}^1 d\rho\ E(\rho)\epsilon_+(\rho)\frac{d\sigma}{d\rho}(\rho)(1+P_eP_\gamma A_l(\rho)), \tag{3.21}$$

$$E_- = \mathcal{L}_-T_-\int_{\rho_{min}}^1 d\rho\ E(\rho)\epsilon_-(\rho)\frac{d\sigma}{d\rho}(\rho)(1-P_eP_\gamma A_l(\rho)), \tag{3.22}$$

The statistical uncertainty $dE_\pm$ comes from the fluctuation in the measured number of events $\frac{dN_\pm}{d\rho}$

$$\frac{dN_\pm}{d\rho} = \mathcal{L}_\pm T_\pm\epsilon_\pm\frac{d\sigma}{d\rho}(1\pm P_eP_\gamma A_l), \tag{3.23}$$

$$dE_\pm^2 = \frac{1}{2}\mathcal{L}T\int_{\rho_{min}}^1 d\rho\ E^2\epsilon_\pm(\rho)\frac{d\sigma}{d\rho}(\rho)(1\pm P_eP_\gamma A_l(\rho)), \tag{3.24}$$

The experimental integrated energy asymmetry is related to the electron polarization by

$$A_{exp} = \frac{E_+-E_-}{E_++E_-} = P_eP_\gamma\frac{< EA_l >}{< E >}. \tag{3.25}$$

The electron polarization is thus proportional to the inverse of the energy-weighted mean longitudinal asymmetry and therefore depends on the detection efficiency and

on the detection threshold ρ_{min}.

Chapter 4

Compton Experimental Setup and Equipment

The Compton polarimeter uses a magnetic chicane to displace the incoming electron beam in order to intersect with a laser beam, creating Compton scattering events (See Figure $4-1$). Backscattered photons are emitted in a narrow cone about the direction of the incident electrons. The photon detector, therefore, must be placed on axis with the electron beam. In order to allow for scattered photon and electron detection, a magnetic chicane consisting of four dipole magnets is used to deflect the electron beam from the standard beam direction. The first two magnets of the chicane displaces the electron beam vertically by 57 cm. Within the Compton Polarimeter, a 10W Coherent VERDI laser is sent through a Fabri-Perot cavity where it is reflected many times, increasing the laser power by roughly a factor of 100. The result is about 700-800W of power in the cavity. The electron beam then interacts with the resulting laser at a small crossing angle (1.32°) to create high energy backscattered photons. The last two magnets in the chicane then returns the electron beam back to its nominal path. The four-dipole magnet chicane performs this deflection with no net precession of the electron's spin at the end of the chicane. Table 4 summarises the beam characteristics of the CEBAF electron beam and the 10W Coherent VERDI laser in Hall C.

4.1 Magnetic Chicane

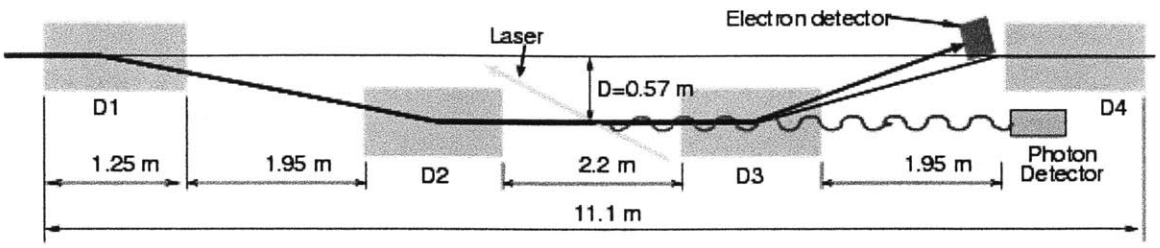

Figure 4-1: Compton Polarimeter Schematic with dipole magnets labelled D1, D2, D3, and D4.

A schematic of the magnetic chicane is shown in Figure $4-1$. The magnetic chicane serves three main purposes. The first is that it must transmit the electron beam achromatically with no changes to the beam dimensions. In other words, the beam leaving the chicane is exactly the same as the beam that enters the chicane. Second, the chicane must allow the laser to intersect with the electron beam. To this end, the first two magnets of the chicane displaces the electron beam downward into the interaction area where a 532nm laser collides with the electron beam. Lastly, the chicane must deflect the scattered electrons away from the main beam. The chicane does this with the third magnet which begins the process of bending the unscattered electrons back to their orginal beam trajectory. Scattered electrons, which have lost energy, will be bent further than the unscattered electrons, separating them from each other. Compton edge electrons (electrons that have lost the most energy) are bent to a maximum distance of 17mm away from the unscattered beam. The design and construction of the 4-dipole chicane, including associated stands and vacuum

Beam energy	[GeV]	1.165
Beam Polarization	[%]	85
Beam Current	[μA]	160
Laser Wavelength	[nm]	532
Laser Power	[W]	10
Cavity Gain	unitless	100
Crossing Angle	°	1.32

Table 4.1: Hall C beam and laser characteristics

chambers were carried out at MIT-Bates.

Table 4.1 summarises the characteristics of the chicane used in Q_{weak}.

Dipole Length	[m]	1.25
Nominal Field	[kG]	5.58
Bend Angle	[°]	10.3
Beam Offset	[cm]	57
Dispersion	[cm/%]	0.43

Table 4.2: Hall C chicane characteristics

4.2 Detectors

Currently, Q_{weak} scattered electron and photon data is collected with the use of a diamond strip electron detector and a GSO photon detector respectively. Orginally, photons were to be detected using the MIT-Bates CsI photon detector; however, due to some issues with phosphorescence, Q_{weak} has temporarily adopted the Hall A GSO photon detector into its data acquisition. Investigations are continuing in order to create a long term solution for future photon detection.

4.2.1 Diamond Strip Electron Detector

The electron detector used in Q_{weak} is a 21mm x 21mm chemical vapor deposition (CVD) diamond microstrip (see Figure $4-2$ and $4-3$). Q_{weak} uses 4 planes of the detector in order to increase position resolution. Each plane is separated by approximately 1cm and staggered 100μm with respect to each other. Each plance contains 96 horizontal diamond strips (polycrystalline CVD diamond). The strips are separated by 20μm with each strip being 180μm wide. Metalization on each plane was done with Titanium-Platinum-Gold (TiPtAu).

The electron detector is located between the third and fourth dipole in the chicane, 4 inches in front of the fourth dipole. The bottom edge of the detector is aligned 0.5cm from the primary beam. The third dipole in the chicane, separates unscattered and scattered electrons. Unscattered electrons are bent by the fourth dipole which bends

them back into the original beam trajectory (trajectory before the beam entered the chicane). Scattered electrons, on the other hand, have lost energy and will be bent further, into the electron detector (See Figures $4-1$). An electron is detected once it travels to and interacts with a strip in the electron detector. The relative energy of the detected electrons can be determined by which strip detected the electron. Lower energy electrons are bent further, and they will interact with strips that are further away from the beam. Electrons at the Compton edge (that have lost the most energy), are displaced 17mm from the primary beam. The detectors are oriented such that higher strip numbers correspond to lower energy electrons (electrons that lost more energy in scattering).

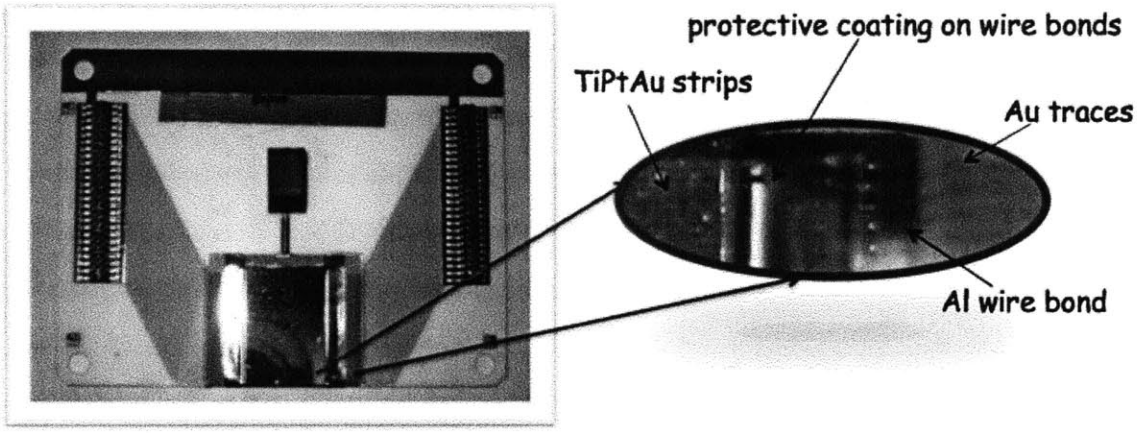

Figure 4-2: Photograph of typical diamond strip detector. Taken from Hall C Polarimetry Wiki [8].

4.2.2 GSO Photon Detector

The photon detector currently in use is a photon calorimeter borrowed from Hall A. The calorimeter uses a cylindrical GSO (Gd_2SiO_5) crystal with a diameter of 6cm and a length of 15cm. Compton photons cause scintillation in the crystal. The scintillation light is then detected by photomultipler tubes. The operations and behavior of the GSO detector is well understood due its use in previous experiments in Hall A.

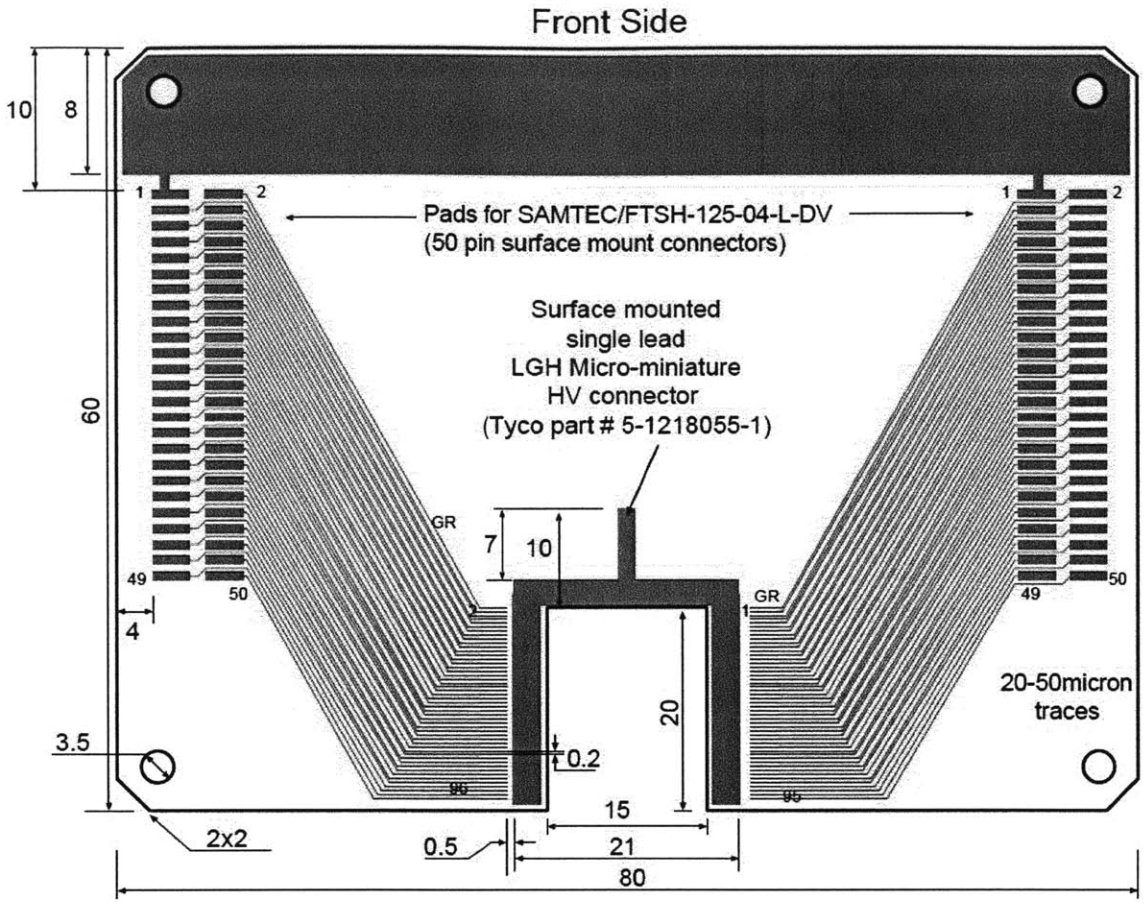

Figure 4-3: Design schematic of diamond strip electron detector. Length measurements are given in mm. Schematic taken from Hall C Polarimetry Wiki [8].

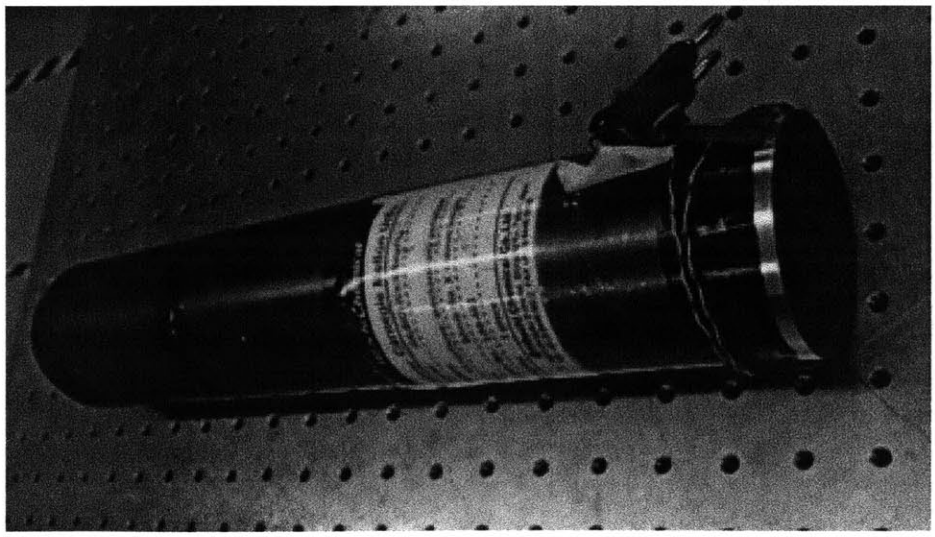

Figure 4-4: Photograph of GSO photon calorimeter. Taken from Hall A Annual Report [6].

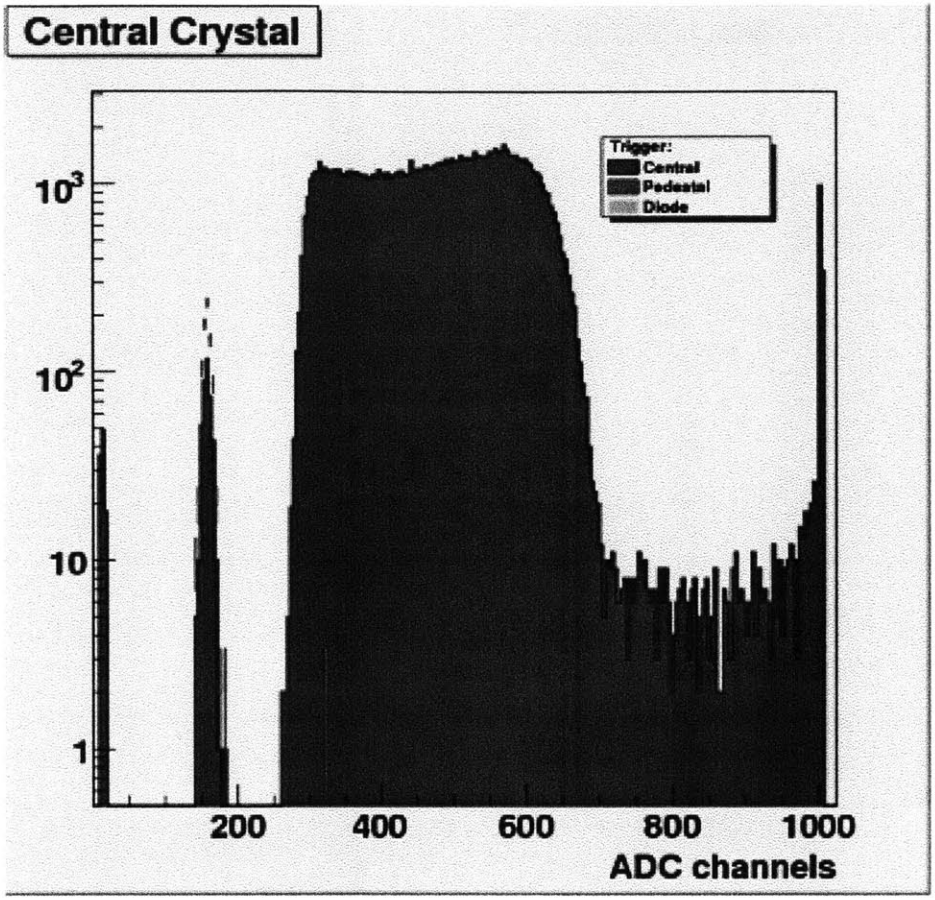

Figure 4-5: Compton scattering sprectrum from previous GSO Calorimeter tests in Hall A. This spectrum was obtained from scattering of 5.9 GeV electrons on a 1064nm laser, and demonstrated a signal-to-background ratio of more than a 100. Note that signals above channel 700 are noise. The Compton edge, corresponding to the highest energy photons, is the quick drop off located on the right side of the central peak. The half-max value is located approximately at channel 650. Plot taken from Hall A Annual Report [6].

Chapter 5

Data and Preliminary Results

Q_{weak} has been collecting Compton data since October 2010. Although the necessary hardware and software for the Q_{weak} precision measurement still requires additional testing and development, current data and analysis has already been developed far enough to produce preliminary measurements of the experimental asymmetry and electron polarization. This section will briefly describe the analysis of the Compton data and show examples of typical data from the Q_{weak} Compton polarimeter.

Compton asymmetry data can be collected by detecting either scattered photons or scattered electrons. An integrated energy spectrum can be obtained using the detected particles from either detector. See Figures $5-1$ and $5-2$ for examples of photon spectra and Figure $5-3$ for an example of an electron spectrum. During a typical run, spectra are recorded with the laser system on and with the laser off. The spectrum taken with laser off represents a background spectrum that can then be used to background-subtract the experimental spectrum (laser on).

Laser on and laser off spectra can be obtained and normalized for both electron helicity states in order to obtain the background-subtracted spectra for each state (See Figures $5-4$ and $5-5$). The energy dependent asymmetry can then be obtained by calculating the difference between the spectra for the two helicity states (See Figure $5-6$ and $5-7$).

The data from many runs can be combined to minimize statistical uncertainties. One method that has already been used to combine the statistics of several runs

is examplified in Figure 5 – 8. Here, an energy weighted asymmetry is calculated for each run and is plotted on the graph. A horizontal line fit can then be used to calculate an average energy weighted asymmetry across these runs.

With knowledge of the theoretical asymmetry and laser polarization, Q_{weak} can use the obtained experimental asymmetry to calculate the electron beam polarization (See Figure 5 – 9).

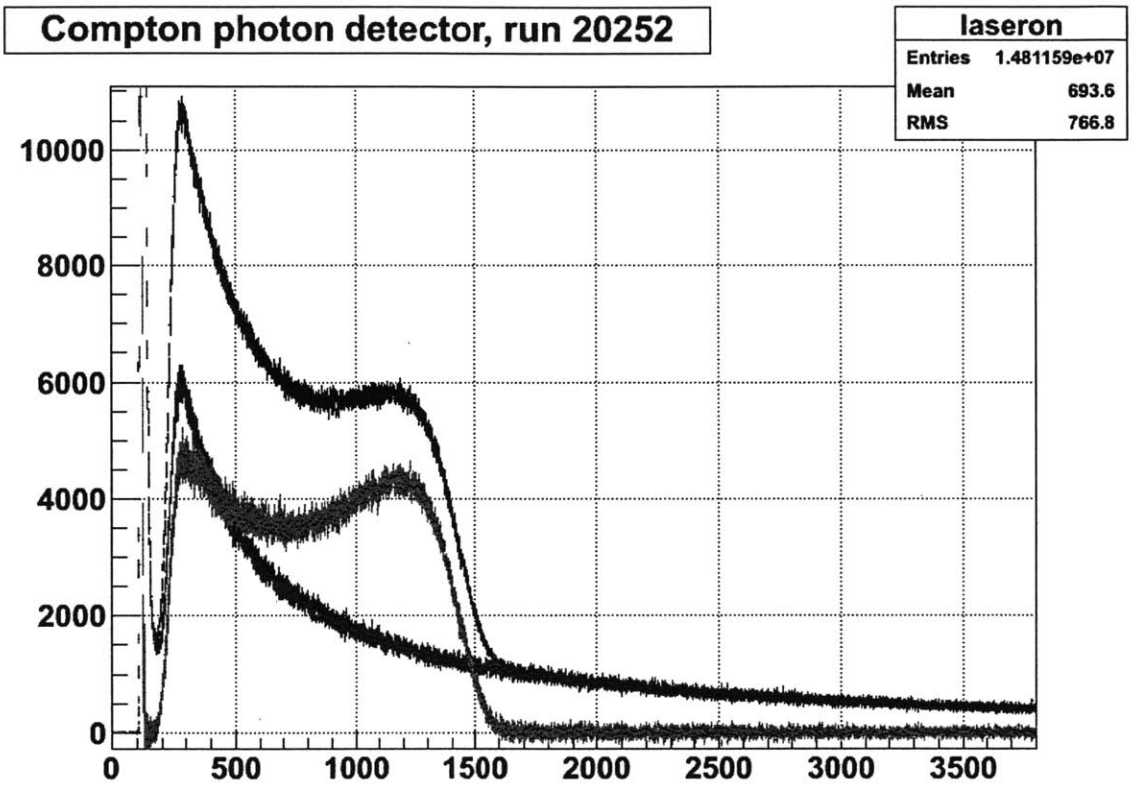

Figure 5-1: Preliminary photon spectrum from the Q_{weak} photon detector. The x-axis is labeled with uncalibrated energy units. The top curve represents the raw photon spectrum. The exponentially decaying curve shows the background spectrum. Finally the lower double-peaked curve shows the background subtracted photon spectrum. Note the Compton edge is manifested as a sudden dropoff on right side of the curve. The Compton edge energy is taken as the half-max value (approximately 1500). Plot taken from Hall C Compton polarimeter run summary webpage [9].

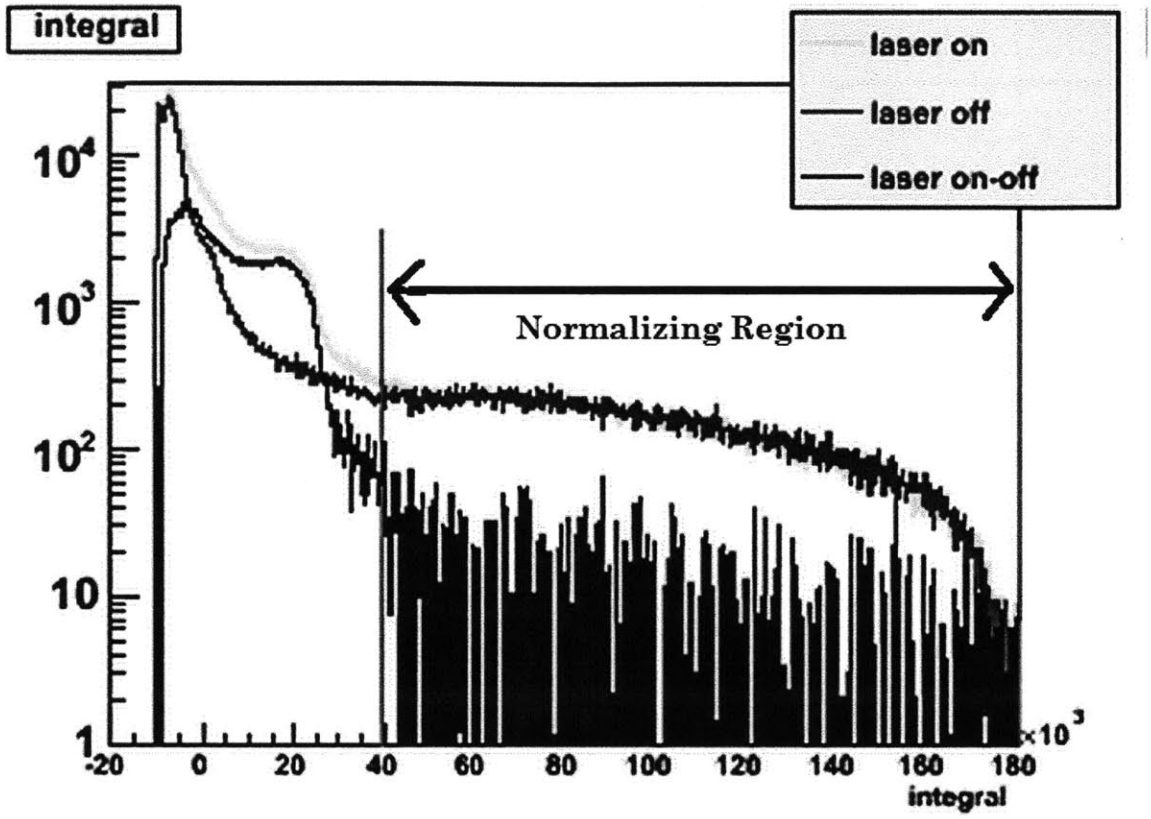

Figure 5-2: Logarithmic integrated spectrum from the photon detector during a typical run. The top (light gray) curve gives the full spectrum with laser on. The second gray curve gives the background spectrum (laser off). The black curve gives the background-subtracted spectrum. The region indicated by the arrows is the region that is used to normalize the spectra with laser on (experimental) and laser off (background) with each other. Here, there is a sudden drop off on the right side of the curve, indicating the Compton edge (highest energy photon). The half-max value is roughly at 25×10^3. Plot taken from Hall C Compton polarimeter run summary webpage [9].

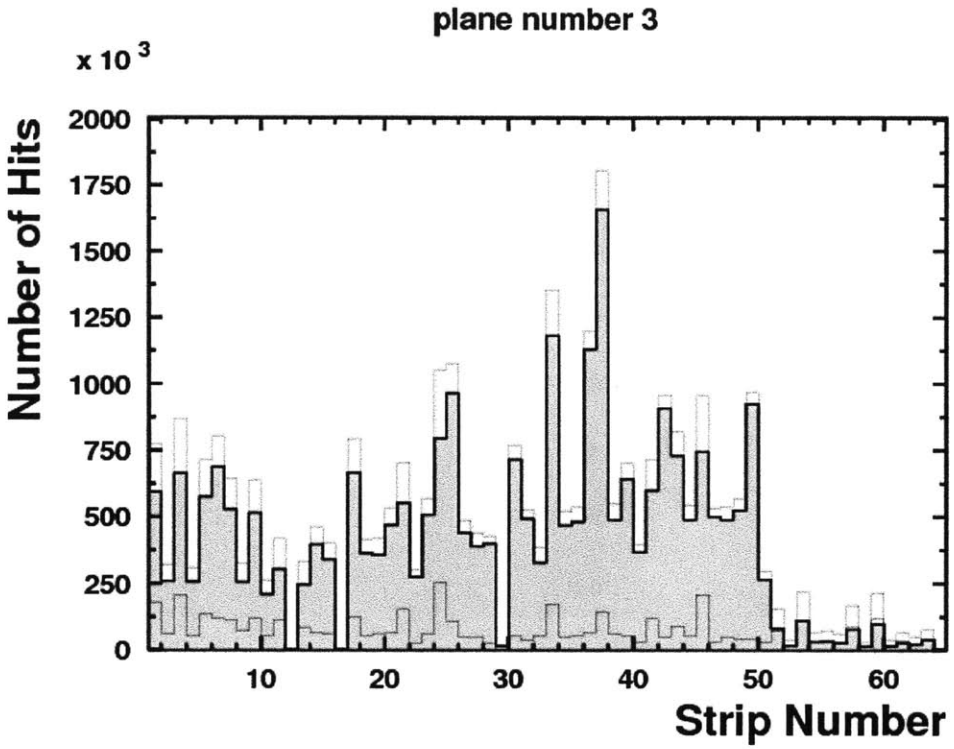

Figure 5-3: Typical background-subtracted spectrum from a plane in the electron detector. Here, there is a sudden drop off on the right side of the curve, indicating the Compton edge (lowest energy electrons). The half-max value is roughly at strip number 50. Plot taken from Hall C Compton polarimeter run summary webpage [9].

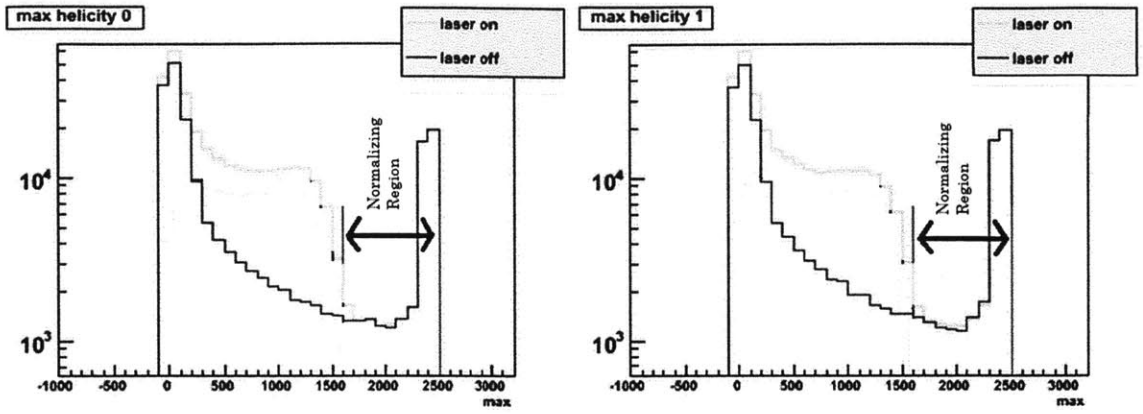

Figure 5-4: Logarithmic spectra separated for each helicity state in a typical run using photon detector data. The top (light gray) curve gives the full spectrum with laser on, while the second (black) exponentially decaying curve gives the background spectrum (with laser off). The regions indicated by the arrows in each graph are the regions that are used to normalize the spectra with laser on (experimental) and laser off (background) with each other. Plot taken from Hall C Compton polarimeter run summary webpage [9].

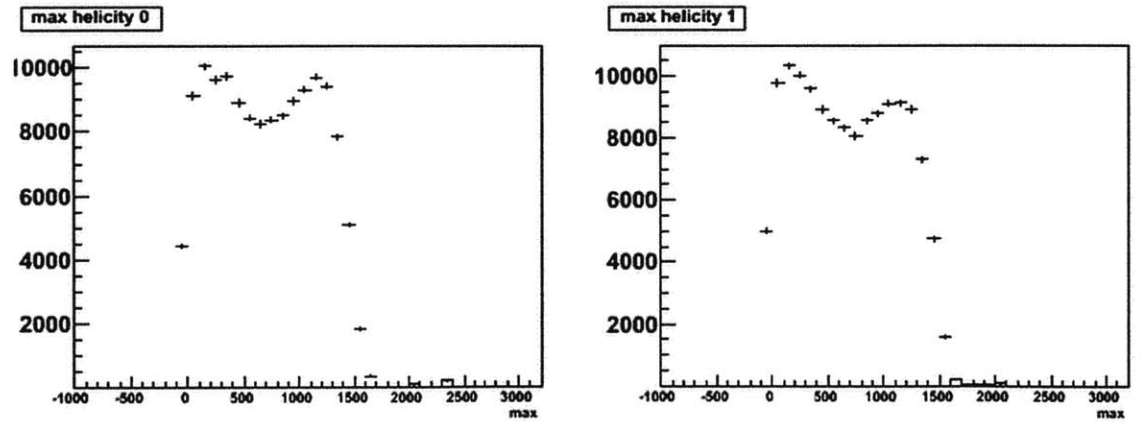

Figure 5-5: Linear background subtracted spectrum of a typical run separated by helicity states (see figures in $5-4$). Spectrum integrated from photon detector data. X-axis is labeled in ADC (uncalibrated energy) units for the scattered photons. The half-max value at the Compton edge in these graphs roughly falls between 1400 and 1500 ADC units. Plot taken from Hall C Compton polarimeter run summary webpage [9].

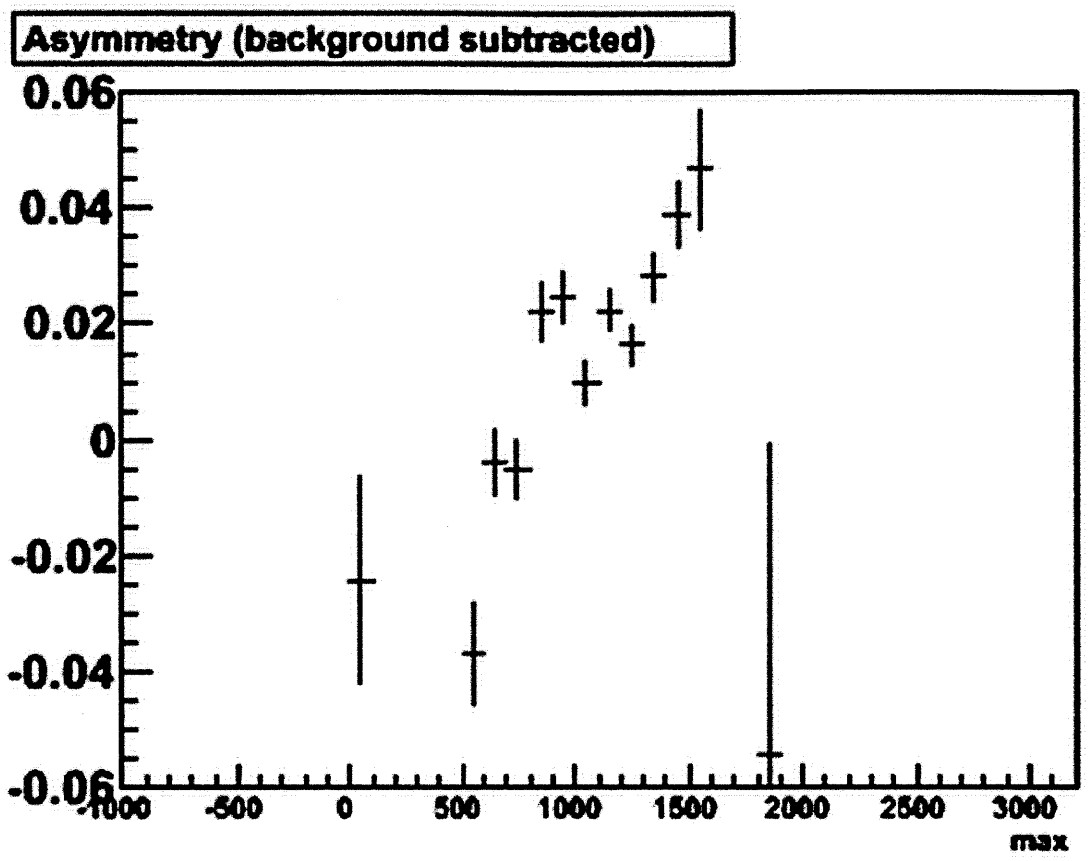

Figure 5-6: Background subtracted asymmetry from photon detector spectra for a typical run (difference between figures in $5-5$). X-axis is labeled in ADC (uncalibrated energy) units for the scattered photons. Note that, consistent with theory, at low scattered photon energy, the asymmetry is negative and becomes positive at high scattered photon energies. The Compton edge is roughly between 1400 and 1500 ADC units which corresponds nicely to the predicted asymmetry of 0.04. Plot taken from Hall C Compton polarimeter run summary webpage [9].

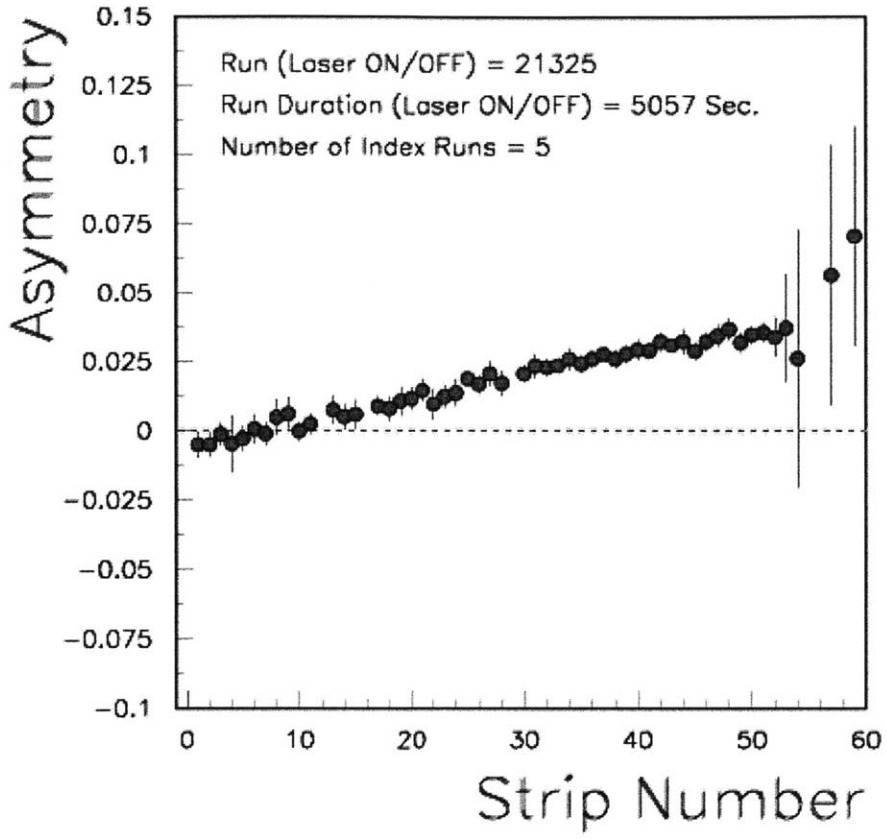

Figure 5-7: Electron detector data from a typical run plotting asymmetry as a function of strip number in the detector. Scattered electrons that lose more energy (and correspond to higher scatterred photon energy) will be bent further and correspond to higher strip numbers. Note that as predicted, low strip numbers (i.e. high scattered electron energy and low scattered photon energy) the asymmetry is negative and becomes positive at high strip numbers (i.e. low scattered electron energy and high scattered photon energy). The Compton edge is located approximately at strip number 55. Plot taken from Hall C Compton polarimeter run summary webpage [9]. Analysis is by V. Tvaskis.

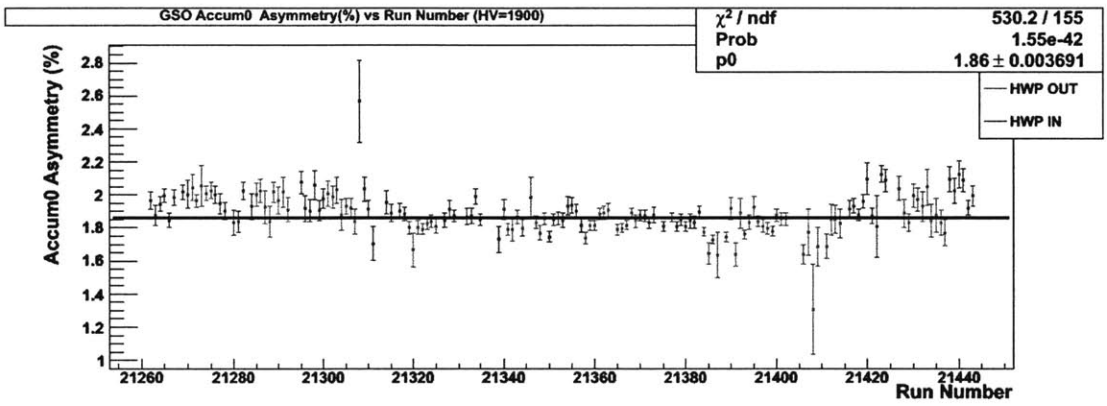

Figure 5-8: Plot of energy weighted asymmetries across multiple runs. The horizontal line represents a horizontal fit indicating the energy weighted average asymmetry for these runs. Plot taken from Hall C online elog [9].

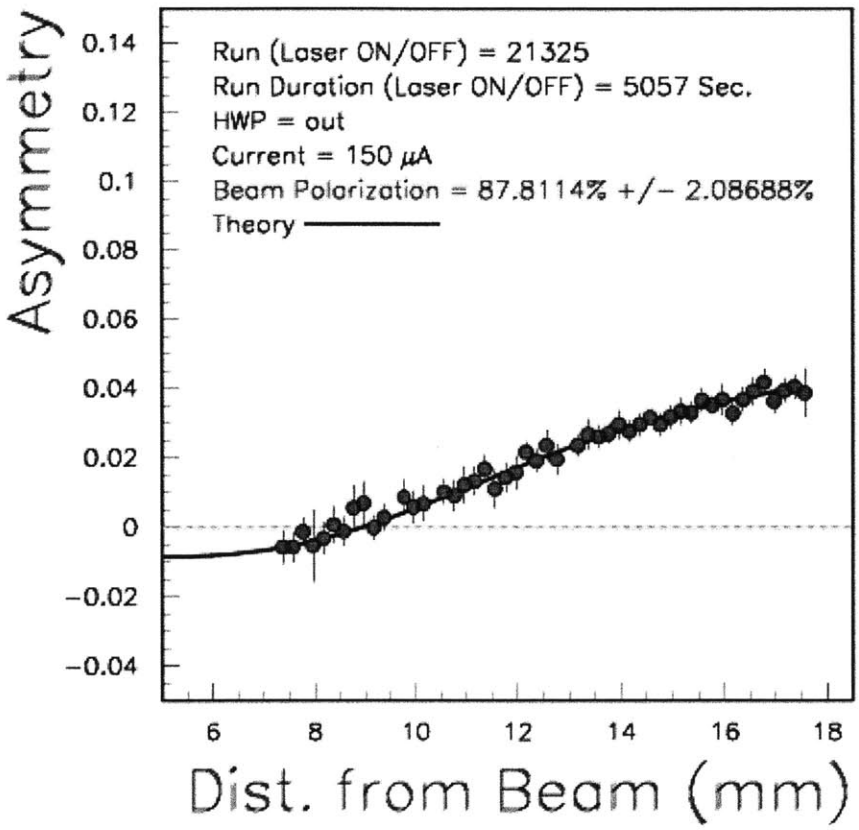

Figure 5-9: Electron detector asymmetry data plotted as a function of the deflected scattered electron's distance from the unscattered beam. Also plotted is a curve representing the expected theoretical asymmetry. The calculated electron polarization here is 87.8%± 2.1%. Plot taken from Hall C Compton polarimeter run summary webpage [9]. Analysis is by V. Tvaskis.

Chapter 6

Conclusions

The Q_{weak} experiment built and installed a new Compton polarimeter in Hall C in order to precisely measure the electron beam polarization for the high-precision Q_W^p measurement. For the experiment, there are three important features of Compton polarimetry:

- The ability to collect data with no changes to the beam dimensions
- Simultaneous running while taking data
- Functionality even at the experiment's high currents (up to $180\mu A$)

These features allow the Compton polarimeter to continuously measure electron beam polarization during the Q_{weak} physics experiment.

Current Compton data collection and analysis systems are already capable of producing measurements of experimental asymmetry and electron polarization. Preliminary results give a electron beam polarization measurement of $87.8\% \pm 2.1\%$. Thus far, Q_{weak} has confirmed proper Compton polarimeter behaviors for operating beam currents as high as $160\mu A$. While many hardware and software systems still require further development in order to reduce and determine statistical and systematic errors, these preliminary results (See Section 5) give a good indication that the Q_{weak} Compton polarimeter will be able to support these developments in order to reach the Q_{weak} precision goals.

Bibliography

[1] D.S. Armstrong et al., "'The Qweak Experiment: A Search for New Physics at the TeV Scale via a Measurement of the Proton's Weak Charge"', Jefferson Lab, Newport New, VA, (2007).

[2] D.C. Jones, "'Development of a Non-invasive, Continuous Polarimeter for Hall C at Jefferson Lab"', *APS April Meeting.* Lecture conducted from APS meeting in Anaheim, CA, (2011).

[3] M. Dalton, "'Compton Photon Detector Update"', *Qweak Collaboration Meeting.* Lecture conducted from Jefferson Lab, Newport News, VA, (2011).

[4] W. Deconinck, "'A Precise Compton Polarimeter for Hall C at Jefferson Lab"', *APS April Meeting.* Lecture conducted from APS meeting in Washington, D.C., (2010).

[5] G. Bardin et al., "'Conceptual Design Report of a Compton Polarimeter for Cebaf Hall A"', Jefferson Lab, Newport News, VA, (1996).

[6] G. Ron et al., "'Hall A Annual Report-2009"', Jefferson Lab, Newport News, VA, (2009).

[7] G. Bardin, C. Cavata, and J-P Jorda, "'Compton Polarimeter Studies for TESLA"', CEA, Saclay, France, (1997).

[8] "'Compton Polarimeter"', *Hall C Polarimetry Wiki*, Retrieved April 29, 2011, from https://hallcweb.jlab.org/polwiki/index.php/Compton_Polarimeter.

[9] *Hall C Polarimeter*, Jefferson Lab, Retrieved April 29, 2011, from https://hallcweb.jlab.org/compton/.

[10] P. Adderley, "'Polarized Injector and Upgrade Schedule"', *Qweak Collaboration Meeting*. Lecture conducted from Jefferson Lab meeting in Newport News, VA, (2009).

[11] S.C. Bennett and C.E. Wieman. and J-P Jorda, *Physics Review Letter*, 82:2484-2487, (1999).

[12] P.L. Anthony et al., *Physics Review Letter*, 95:081601 (2005).

[13] G.P. Zeller et al., *Physics Review Letter*, 88:091802 (2002).

[14] W.M. Yao et al., *Journal of Physics*, G33:1-1232. (2006).

[15] W. Deconinck, William and Mary/Jefferson Lab, Private Communication.

[16] D. Gaskell, Jefferson Lab, Private Communication.

[17] E. Ihloff, MIT-Bates, Private Communication.

[18] D.C. Jones, Jefferson Lab, Private Communication.